Supplementary information

XPCS at elevated pressure and cryogenic temperatures: Multicomponent dynamics in amorphous ice

Aigerim Karina[1,*], Hailong Li[2,3,*], Tobias Eklund[2,4,5], Marjorie Ladd-Parada[6], Bernhard Massani[7], Mariia Filianina[1], Neha Kondedan[1], Andreas Rydh[1], Klara Holl[2,4], Ryan Trevorah[8], Simo Huotari[8], Robert Bauer[9,10], Claudia Goy[9], Nele N. Striker[9], Francesco Dallari[9,+], Fabian Westermeier[9], Michael Sprung[9], Felix Lehmkühler[9,11], Katrin Amann-Winkel[2,4,1,#]

[1]Department of Physics, Stockholm University, Sweden
[2]Max-Planck-Institute for Polymer Research, Germany
[3]State Key Laboratory of Fine Chemicals, School of Chemical Engineering, Dalian University of Technology, China
[4]Institute of Physics, Johannes Gutenberg University Mainz, Germany
[5]European X-ray Free-Electron Laser, Germany
[6]Department of Chemistry, Glycoscience Division, KTH, Stockholm, Sweden
[7]The University of Edinburgh, School of Physics and Astronomy (SoPA), Centre for Science at Extreme Conditions (CSEC), Edinburgh, UK
[8]Department of Physics, University of Helsinki, Finland
[9]Deutsches Elektronen-Synchrotron DESY, Germany
[10]Freiberg Center for Water Research, Technische Universität Bergakademie Freiberg, Germany
[11]Hamburg Centre for Ultrafast Imaging, Germany

#Corresponding author. Email: amannk@mpip-mainz.mpg.de

*These authors equally contribute to this work.

+ Currently at: Department of Physics and Astronomy, University of Padova,

Introduction

The pressure dependence of the glass transition provides insight to relaxation dynamics and related viscosity changes at elevated pressure. This is of particular interest for the glassy states of water, where two amorphous states of different density exist. We present novel X-ray photon correlation spectroscopy (XPCS) experiments at elevated pressure and cryogenic temperatures using a diamond anvil cell (DAC). Extended fit procedures and additional data are summarized as follows.

Samples

We have measured in total five equilibrated high-density amorphous ice samples (eHDA). All samples have been prepared ex-situ using a piston cylinder setup, following a well-established protocol (see Methods and Materials of the main manuscript). [1], [2] The quench recovered samples have been transported in liquid nitrogen to the beamline. Prior to the experiment, the samples were cold-loaded into a diamond anvil cell (DAC), and carefully repressurized using the four screws on the DAC. The pressure was determined using ruby fluorescence at the lowest temperature.

The samples have been heated in-situ until crystallization or transformation to LDA. The five conditions are summarized in table 1. The ruby system to determine the sample pressure, was only installed successfully for the second beamtime, therefore the pressure for samples G and F was estimated from the position of the eHDA diffraction peak as well as the crystalline phase it transformed to. The transition temperatures and related pressures, derived from the WAXS analysis (Fig. S1), are summarized in the phase diagram in Fig. 7 of the main manuscript.

Sample	Absorber	Pressure (GPa)	Beamtime	
eHDA_A	12	0.08 (Ruby line)	#2 (2022)	
eHDA_B	18	0.08 (Ruby line)	#2 (2022)	
eHDA_G	24	~0.1 (estimated)	#1 (2021)	noisy g_2
eHDA_F	24	>0.25 (estimated)	#1 (2021)	Pseudo-Kossel lines
eHDA_D	18	0.75 (Ruby line)	#2 (2022)	Pseudo-kossel lines

Table 1: Summary of eHDA samples measured by XPCS inside a DAC. "Absorber" describes the number of 25 µm thick silicon foils used as attenuator to mitigate radiation damage. 12 and 18 foils correspond to an X-ray transmission of 0.27 and 0.14 at 12 keV photon energy, respectively. The analysis of the correlation function at the two highest pressures was not possible, due to the appearance of Pseudo-Kossel lines (see section "Experimental setup").

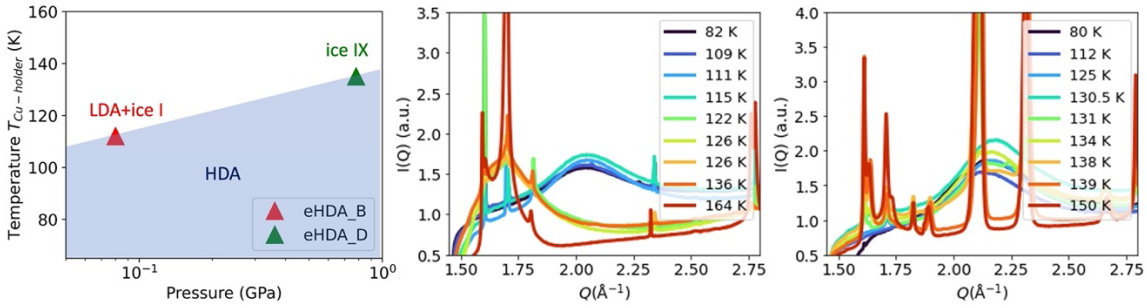

Fig. S1: (Left) Phase diagram depicting the sample temperature and pressure, at which the different samples transformed to LDA, ice Ih and ice IX respectively. XRD pattern for sample B (middle) and sample D (right). The first diffraction maximum of eHDA at 80 K for sample D is clearly distinct (Q = 2.2 Å^{-1}) due to the higher pressure (0.75 GPa). This sample directly crystallizes to ice IX at T_{cryo} = 135 K (T_{sample} = 150 K).

Experimental setup and temperature calibration

A picture of our experimental setup is shown in Fig. S2a, and consist of a cubic vacuum chamber, a cryostat and a ruby fluorescence setup. Details are summarized in the main manuscript in the Methods section, additional information is provided here. To measure the pressure of the sample inside the DAC while mounted to the beamline, we used a rotational flange (VAb DDF 100P) between the cold finger and the vacuum chamber. This allows us to determine the pressure before and after the XPCS experiments by rotating the cold finger 90 degree off and making the DAC facing the ruby fluorescence setup (Fig. S2A, number 5).

DAC was clamped by a two-part Cu block via screws (Fig. S2B). Since there remains a small gap between Cu-block and DAC, in particular for cold-loading procedures, the thermal contact between copper holder and DAC is not perfect. This leads to a temperature offset between the measured temperature during the experiment (T_{cryo}) and the sample compartment inside the DAC (T_{sample}). During the experiments, the temperature (T_{cryo}) at the bottom of the cryostat is measured using a Si-diode (Fig. S2B). After the X-ray experiments, we calibrated this offset by gluing a thermocouple onto the gasket inside the DAC. The results for the cooling are shown in Figure S3. After several cycles of various measurements, the temperature offset was determined to be 15 ± 2 K.

As the X-ray beam penetrated through the two diamond anvils, Pseudo-Kossel-lines were observed on the detector. The image in Fig. S2C shows a strong line visible at a pressure of 0.75 GPa in the 2D SAXS pattern. Small Pseudo-Kossel lines can also be observed in 2D WAXS pattern (Fig. 1A), but do not affect the WAXS analysis. The XPCS analysis, however, is done from the SAXS images, and strong Pseudo-Kossel lines affect the calculated correlation function, even after masking the relevant pixels. For the here described first experiments, we used type Ia diamonds. Later experiments indicated that this effect can be reduced by the use of type IIa diamonds.

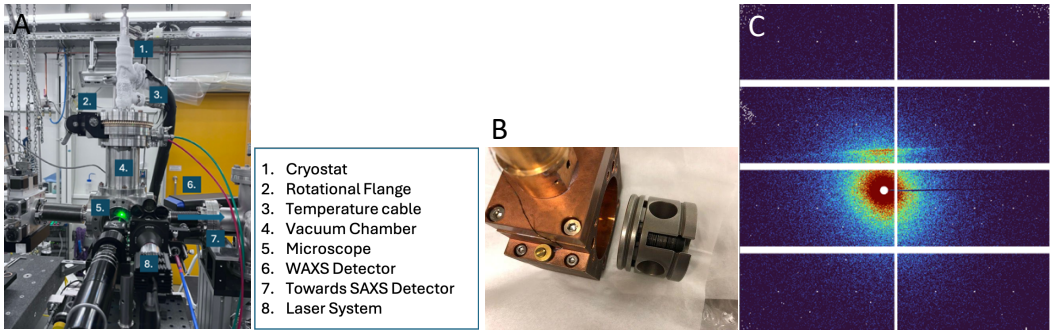

Fig S2: A) Customized experimental setup at beamline P10 (PETRA III, DESY). B) Cold-head with Cu-sample holder and DAC. C) SAXS detector image with strong Pseudo-Kossel line.

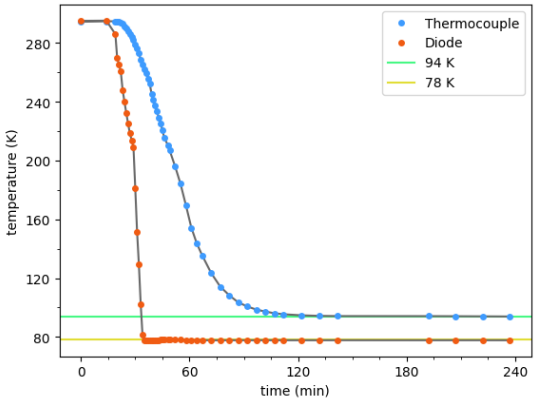

Fig. S3: Temperature calibration measurement to quantify the offset between cryostat finger and sample compartment.

Sample A

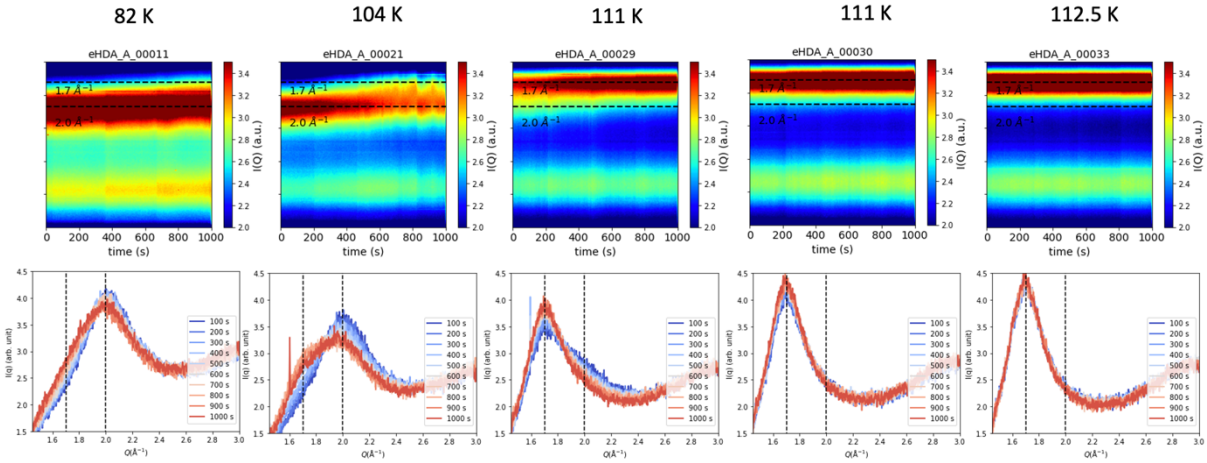

Fig. S4: Wide angle X-ray scattering intensity. The time evolution of the first diffraction maximum for sample A is plotted.

Figure S5, top row, shows the g_2 functions and the related fits at different Q. In the bottom row, the fit results for the Kohlrausch–Williams–Watts (KWW) exponent γ are shown. This is related to Figure 2 in the main manuscript.
In Fig 3 of the main manuscript the two-time correlation functions (TTC) of the first 300 s of experimental time are displayed. In total we measured 1000 scattering patterns, each pattern was exposed to X-rays for 1s. The TTCs for the complete 1000 s are shown in Fig. S6.

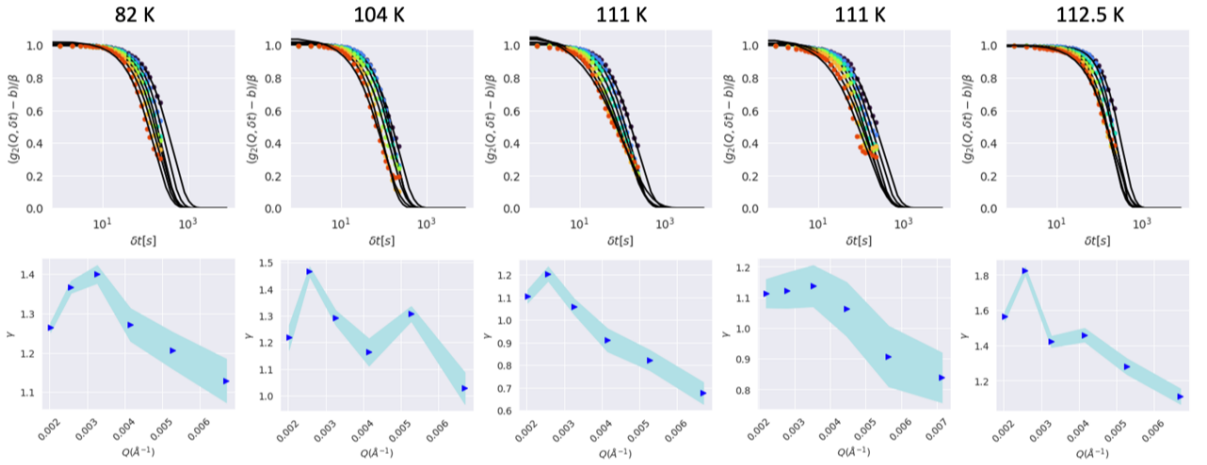

Fig. S5: (Top row) Autocorrelation functions g_2 and the corresponding Kohlrausch–Williams–Watts (KWW) fits for sample A. (Bottom row) fit results for the KWW exponent γ.

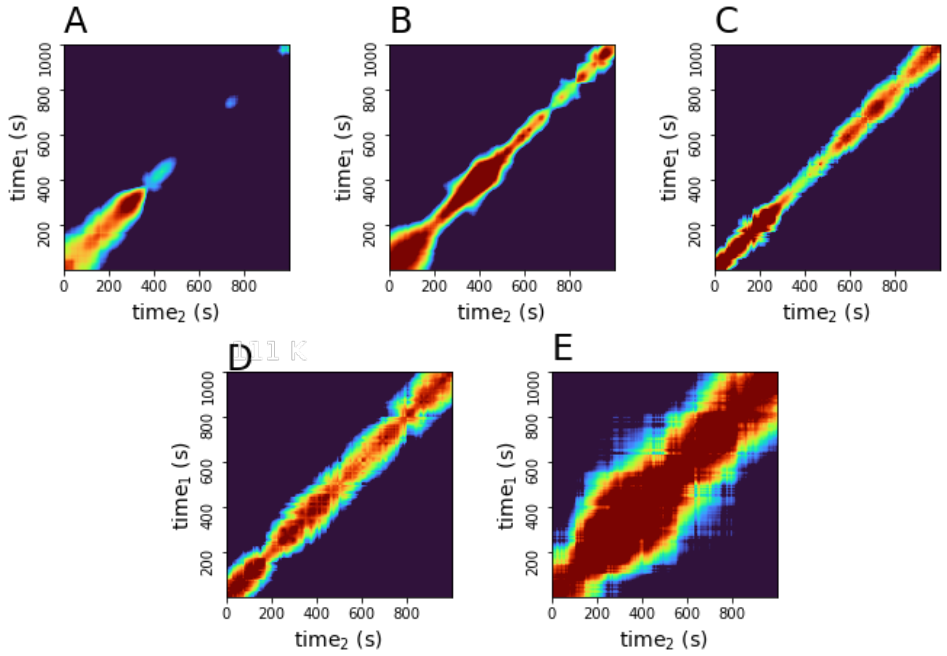

Fig. S6: Two-time correlation functions for sample A at Q = 0.0033 $Å^{-1}$ and at temperatures T_{cryo} = 82 K, 104 K, two times 111 K at two different sample positions, and 112.5 K.

Sample B

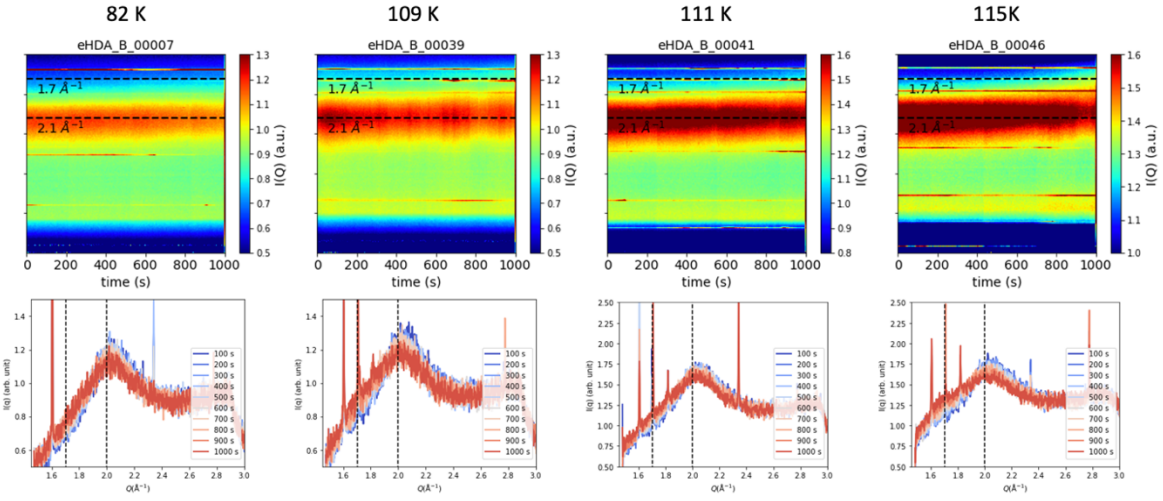

Fig. S7: Wide angle X-ray scattering intensity. The time evolution of the first diffraction maximum for sample B is plotted.

In the main manuscript we discussed that the correlation functions of sample B (Fig. 5) can be best modelled by simultaneously fitting two dynamical components (see Fig. 6). We additionally tested a single exponential KWW decay fit using Equation (3) of the main manuscript, the results are shown in Fig. S8. The middle row shows the corresponding KWW-exponent (γ) of the KWW fit. The Q-dependencies of the relaxation time (τ) are shown in the lower row. It is evident from this figure that a single (diffusive) component cannot fit the data, as the relaxation times do not display a clear Q^2-dependence, the fit rather exhibits a clear offset. Therefore, a multicomponent fit was applied in the main manuscript.

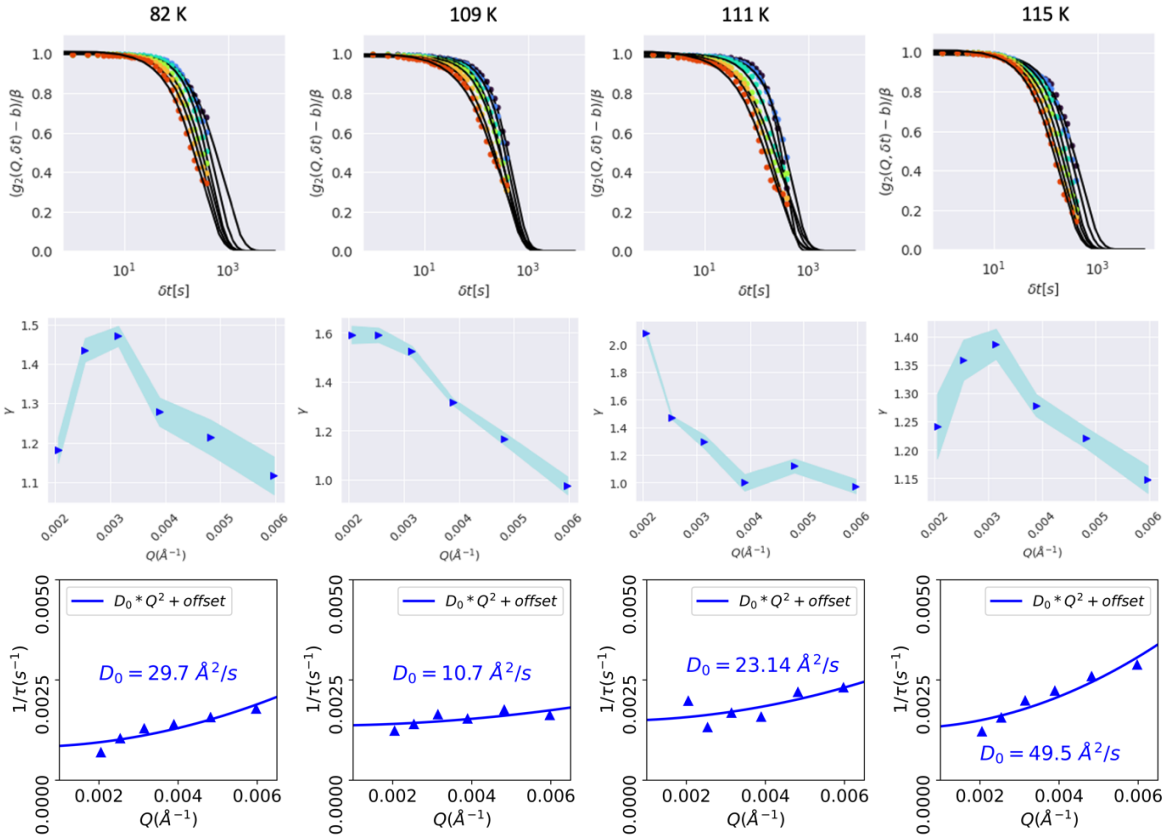

Fig. S8: (Top row) Autocorrelation functions g_2 and the corresponding KWW fits of sample B, calculated for the first 500 s of a series at Q = 0.0035 Å^{-1}. (Middle row) The results for the KWW exponent of fitting the g_2 functions of sample B. (Lower row) Q-dependency of the relaxation time τ.

1. Winkel, K., et al., *Water Polyamorphism: Reversibility and (Dis)continuity.* Journal of Chemical Physics, 2008. **128**(4): p. 6.
2. Mariedahl, D., et al., *X-ray Scattering and O–O Pair-Distribution Functions of Amorphous Ices.* The Journal of Physical Chemistry B, 2018. **122**(30): p. 7616-7624.